

AXISYMMETRIC AND NON-AXISYMMETRIC FLOW AND WALL SHEAR STRESS IN A MODEL FUSIFORM ABDOMINAL AORTIC ANEURYSM

Gregory J. Sheard

Fluids Laboratory for Aeronautical and Industrial Research (FLAIR), Department of Mechanical and Aerospace Engineering, Monash University, VIC 3800, Australia, Greg.Sheard@eng.monash.edu.au

ABSTRACT

Pulsatile flow through a sinusoidal bulge in an otherwise straight circular tube is used to model the fluid mechanics within a fusiform abdominal aortic aneurysm. Three-dimensional flow is computed using a high-order spectral-element/Fourier method, driven by an anatomically realistic heartbeat waveform. Model dimensions and parameters are chosen to describe human abdominal aortic aneurysms considered both low and high risk in terms of their likelihood of rupture. A Reynolds number of 330, a Womersley number of 10.7, and aneurysm length and diameter ranges of 2.9-5.2 and 1.3-2.1 times the vessel diameter, respectively, are investigated. Variation in wall shear stress with both time and as a function of aneurysm dimension is computed. From computations on a bulge with maximum diameter approximately twice the undilated tube diameter, the flow is found to be naturally three-dimensional under conditions consistent with the human abdominal aorta. However, the dominant feature of the flow remains an axisymmetric vortex ring, which is generated at the proximal end of the bulge during systole. Both three-dimensional flow and non-uniformity in azimuthal wall-shear-stress distribution are most pronounced in the vicinity of the distal end of the bulge during the resting phase of the heartbeat. The axial distribution of wall shear stress scales approximately with the length of the bulge. The flow is sensitive to changes in the bulge diameter: a bulge with maximum diameter 1.9 times the vessel diameter invokes significantly more complex dynamics than a modest bulge of 1.3 diameters.

Key Words: *blood flow, wall shear stress, aneurysm, three-dimensional transition, spectral-element method.*

1 INTRODUCTION

Aneurysms present as a localized enlargement of an artery, caused by weakness or degradation in the tissue integrity comprising the artery wall.^[1,2] Recent attention has focused on the role of blood flow on aneurysm mechanics, characterizing the fluid mechanics within an aneurysm, and determining the fluid stresses imparted on the artery and aneurysm walls. Recent experiments^[3] and axisymmetric simulation^[4] have shown that in fusiform aneurysms, the flow is dominated by a strong vortex ring, which develops in the bulge during the systolic phase of the heartbeat waveform. This study employs three-dimensional analysis and simulation to investigate three-dimensional features of this complex flow system.

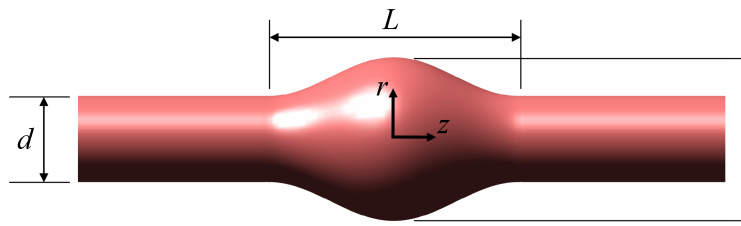


Figure 1: A schematic diagram of the fusiform aneurysm model, with cylindrical r - z coordinate system and dimensions shown.

2 METHODOLOGY

In this study, the aneurysm is modeled as a sinusoidal bulge in an otherwise straight pipe,^[4] characterized by a length ratio $LR = L/d$ and a diameter ratio $DR = D/d$, where L is the aneurysm bulge length, d is the undilated tube diameter, and D is the maximum bulge diameter. Flow is driven by a pressure gradient derived to reproduce a physiologically realistic pulse waveform. A Reynolds number based on the time-averaged mean velocity through the model (U) is defined as $Re = Ud/\nu$, where ν is the kinematic viscosity of the fluid. In this study a Reynolds number of $Re = 330$ is chosen consistent with previous studies. Similarly, a Womersley number of $\alpha = 10.7$ is employed ($\alpha = \frac{d}{2}\sqrt{2\pi f/\nu}$, where f is the frequency of the heartbeat). Two-dimensional flow and linear stability analysis were computed using an incompressible Navier–Stokes solver^[4,5] based on the spectral-element method.^[6] Three-dimensional computations were efficiently calculated using a spectral-element/Fourier algorithm detailed in Blackburn & Sherwin.^[7]

3 RESULTS: 3D FLOW DEVELOPMENT

Using a Floquet linear stability analysis technique formulated in cylindrical coordinates,^[5] the axisymmetric flow computed and described in Sheard^[4] was analysed at a range of Reynolds numbers to determine the stability of the pulsatile flow to non-axisymmetric perturbations. The fastest-growing wavenumber was found to change with Reynolds number: the flow was predicted to first become unstable with a wavenumber $m = 1$ at $Re \approx 270$. Inspection of the perturbation field arising from this analysis demonstrated that the non-axisymmetric flow features evolved in the distal region of the bulge during the resting phase of the heartbeat, before being flushed out of the bulge during the systolic phase. At $Re = 330$, matching Salsac *et al.*^[3] and Sheard^[4], who selected parameters relevant hemodynamics within a human abdominal aorta, the fastest-growing wavenumber was $m = 3$, though the location and behaviour of the three-dimensional structures was similar to that at onset of the transition.

Three-dimensional simulations were then conducted to confirm these predictions at $Re = 330$. Figure 2 plots contours of wall shear stress magnitude over single a period from the saturated three-dimensional simulation. The contours indicate that the non-axisymmetric effects are most visible in the resting phase of the pulse cycle (*a*). During the systolic phase (*c*), where wall shear stress levels are highest, there is little wall shear stress variation in the azimuthal direction: axisymmetric features dominate.

4 RESULTS: GEOMETRY VARIATION

Consideration was given to the effect of changing the aneurysm geometry on the distribution of wall shear stress magnitude ($|wss|$), taken as the leading eigenvalue of the rate-of-strain tensor: the wall shear

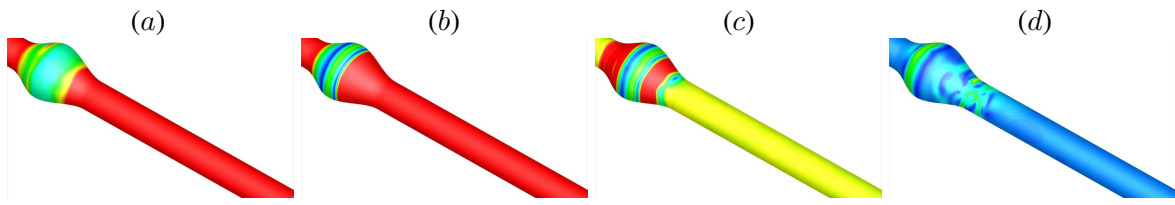


Figure 2: Flooded contours of wall shear stress magnitude ($|\text{WSS}|$) plotted on the surface of the aneurysm model with $\text{LR} = 2.9$ and $\text{DR} = 1.9$. The model is shown in isometric view with flow from left to right. The frames are taken at equi-spaced times during the pulse cycle: (a-b) displays the resting (diastolic) phase, and (c-d) shows the systolic phase. Contour levels from 0 (blue) through to $40U/d$ (red) are plotted.

stress is recovered by multiplying these dimensionless values by $\mu U/d$). Motivated by the previous observation that $|\text{WSS}|$ is predominantly axisymmetric in this model aneurysm, axisymmetric simulations were undertaken to investigate how $|\text{WSS}|$ throughout the model varied in time. The plots in figure 3 show contours of $|\text{WSS}|$ in t - z space: that is, along any horizontal line the axial $|\text{WSS}|$ distribution along the vessel and aneurysm wall is given at that instant in time. A single heartbeat is shown.

In figure 3(a), the length ratio is varied over $2.9 \leq \text{LR} \leq 5.2$ for a constant diameter ratio $\text{DR} = 1.3$. It is notable that the $|\text{WSS}|$ is similarly distributed in these plots (peak systole occurs at approximately $t = 0$), and away from the aneurysm bulge, the wall shear stress is axially uniform and consistent irrespective of LR . Within the bulge ($|z|/d < 1.45, 1.95$ and 2.6 for top, middle and bottom, respectively), a high zone of $|\text{WSS}|$ is detected in the vicinity of $z/d = 1.5$ - 2 at $t \approx 0$, followed by a localized peak of $|\text{WSS}|$ which migrates upstream over $0.1 \lesssim t/T \lesssim 0.3$ from just upstream of the centre of the aneurysm bulge ($z \approx 0$). These correspond to the flushing of fluid into the distal artery at systole, and the development of a secondary vortex ring after peak systole (as described in Salsac *et al.*^[3] and Sheard^[4]). With increasing length ratio, the magnitude of $|\text{WSS}|$ within the bulge decreases, and the distribution appears to scale in the axial direction with the length ratio.

To consider diameter-ratio variation, three models with $\text{LR} = 2.9$ and $\text{DR} = 1.3, 1.9$ and 2.1 were studied (figure 3(b)). It was found increasing the diameter ratio leads to a marked change in $|\text{WSS}|$ distribution. At higher diameter ratios, the regions of highest $|\text{WSS}|$ are consistently located in the distal half of the bulge and into the distal artery. In contrast to the smaller diameter ratio $\text{DR} = 1.3$, for $\text{DR} \gtrsim 1.9$, the aneurysm bulge experiences $|\text{WSS}|$ levels far higher than recorded in the undilated artery segments, and these persist for a majority of the heartbeat cycle. Even during the resting phase, elevated $|\text{WSS}|$ levels are detected in the bulge at $z \approx -0.6$. A further striking difference is the appearance of small regions of low $|\text{WSS}|$ during systole (e.g. see $t \approx 0$ and 0.2), in contrast to the $\text{DR} = 1.3$ cases. This indicates that at larger aneurysm diameters, vessel wall tissue is exposed to greater levels of peak $|\text{WSS}|$, and greater temporal and spatial fluctuations in $|\text{WSS}|$, all of which can erode the integrity of luminal tissue.^[1,2]

5 CONCLUSIONS

A stability analysis and high-resolution non-axisymmetric computations of a flow representative of pulsatile flow through a fusiform human abdominal aortic aneurysm have shown that while the flow is non-axisymmetric under these conditions, wall shear stress is predominantly axisymmetric. By systematically varying the length ratio and diameter ratio independently, it has been found that the axial wall-shear-stress distribution scales approximately with the length of the aneurysm bulge, and that increasing the bulge diameter invokes a marked increase in the spatio-temporal fluctuation of wall shear stress throughout the pulse cycle, due to the increased circulation in the vortex ring shed into the bulge during the systolic phase of the heartbeat.

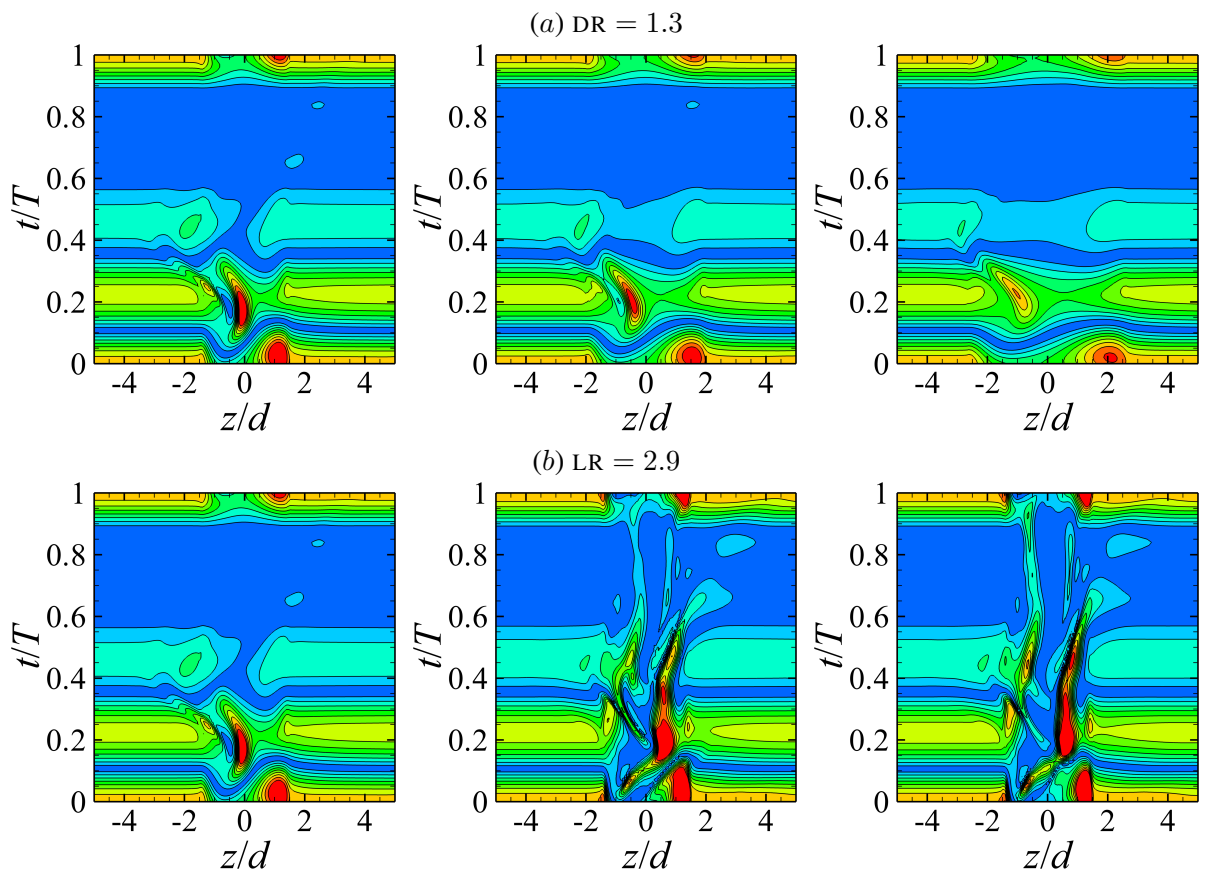


Figure 3: Contours of shear rate plotted on t - z axes to demonstrate the variation in wall shear stress over a single pulse cycle. (a) $DR = 1.3$, and from left to right $LR = 2.9, 3.9$ and 5.2 . (b) $LR = 2.9$, and left to right $DR = 1.3, 1.9$ and 2.1 . 10 equi-spaced contour levels are plotted between 0 (blue) and $100U/d$ (red).

REFERENCES

- [1] J.C. Lasheras, The biomechanics of arterial aneurysms, *Ann. Rev. Fluid Mech.*, **39**, 293-319, 2007.
- [2] R.B. Rutherford, Randomized EVAR trials and advent of level I evidence: a paradigm shift in management of large abdominal aortic aneurysms?, *Semin. Vasc. Surg.*, **19**(2), 69-74, 2006.
- [3] A.-V. Salsac, S.R. Sparks, J.-M. Chomaz and J.C. Lasheras, Evolution of the wall shear stresses during the progressive enlargement of symmetric abdominal aortic aneurysm, *J. Fluid Mech.*, **560**, 19-51, 2006.
- [4] G.J. Sheard, Flow dynamics and wall shear stress variation in a fusiform aneurysm, *J. Eng. Math.*, DOI: 10.1007/h10665-008-9261-z, 2009.
- [5] G.J. Sheard and K. Ryan, Pressure-driven flow past spheres moving in a circular tube, *J. Fluid Mech.*, **592**, 233-262, 2007.
- [6] G.E. Karniadakis, M. Israeli and S.A. Orszag, High-order splitting methods for the incompressible Navier–Stokes equations, *J. Comput. Phys.*, **97**, 414-443, 1991.
- [7] H.M. Blackburn and S.J. Sherwin, Formulation of a Galerkin spectral element-Fourier method for three-dimensional incompressible flow in cylindrical geometries, *J. Comput. Phys.*, **197**, 759-778, 2003.

CMBE09

1st International Conference on Computational & Mathematical Biomedical Engineering

29th June – 1st July, 2009, Swansea University, UK

Edited by:

Perumal Nithiarasu

Civil and Computational Engineering Centre
School of Engineering, Swansea University
Swansea, UK

Rainald Löhner

Center for Computational Fluid Dynamics
College of Sciences, George Mason University
Fairfax, Virginia, US

Raoul van Loon

Civil and Computational Engineering Centre
School of Engineering, Swansea University
Swansea, UK

With support from:

Xianghua Xie, Igor Sazonov, Antonio Orlando, Antonio Gil
Swansea University, Swansea, UK

1st International Conference on Computational & Mathematical Biomedical Engineering,
2009, Swansea, UK

First edition, June 2009

© 2009 by the authors of the abstracts

Published by CMBE

ISBN: 978-0-9562914-0-0

CONTENTS

Keynote Lectures

Constrained mixture models of arterial adaptation: past successes and future promises J.D. Humphrey	3
Towards a comprehensive computational model for the respiratory system W.A. Wall, L. Wiechert, A. Comerford, S. Rausch	4
Multi-Layered soft collagenous tissues: constitutive modeling and inverse analysis G.A. Holzapfel	6
Patient-specific modeling of blood flow and vessel wall dynamics C.A. Taylor	7
Computational modelling of optic nerve head biomechanics C.R. Ethier	8
Modeling collagen (re)modeling F.P.T. Baaijens	9
Clinical application of image-based CFD for cerebral aneurysms J.R. Cebal	10
Wall stress analysis of abdominal aortic aneurysms and its possible use for personalized diagnostics planning F.N. van de Vosse, L. Speelman, M. vant Veer, S. de Putter, E.A. van Dam, E.M.H. Bosboom, M.C.M. Rutten, M. Breeuwer, G.W.H. Schurink, J. Buth	11

MS-1: Advances in arterial wall mechanics and haemodynamics

Organised by J.D. Humphrey, C.A. Taylor and G.A. Holzapfel

Prestressing patient-specific biomechanical problems under finite deformation M.W.Gee, W.A.Wall	15
Computational fluid dynamics: clinical application in human coronary arteries F.Gijssen, J.Wentzel, H.Schuurbiers, A.van der Steen, P.Serruys	19
Unsteady fluid solid interaction analysis of a bifurcation in a human healthy left coronary artery M.Malve, J.F.Rodríguez, A.Garcia, M.A.Martínez, M.Doblare	23
Simulation of blood flow in thoracic aorta for prediction of long-term adverse events H.Suito, T.Ueda, G.D.Rubin	27
A multi-model approach to intravenous filter optimization Y.V.Vassilevski, S.S.Simakov, S.A. Kapranov	31
Towards in vivo identification of cerebral aneurysm wall properties J.Lu, X.Zhao	35
Filtering-based data assimilation in fluid-structure interaction: towards personalization of vascular models C.Bertoglio, M.A.Fernandez, J.-F.Gerbeau, P.Moireau	39

Mathematical and numerical models for healthy and diseased arterial wall M.De Luca	43
How do residual stresses arise in arteries? L.Cardamone, J.D.Humphrey	47

MS-2: Multiphysics multiscale computational modelling of the cardiovascular system

Organised by P.J. Blanco and R.A. Feijoo

Modelling controlled drug release and transport phenomena in the arterial wall S.Minisini, L.Formaggia	51
A 3D fluid-structure interaction non-Newtonian model for blood flow using 1D absorbing boundary conditions A.Moura, J.Janela, A.Sequeira.	55
Massively parallel cardiac computational electrophysiology in anisotropic media R.Aris, G.Houzeaux, M.Vazquez, D.Gil, J.Garcia-Barnes	59
Efficient partitioned procedures for fluid-structure interaction algorithms F.Nobile, C.Vergara	63
Finite Element Methods for a Mesoscopic Constitutive Model of Blood A.Iolov, Y.Bourgault, A.Fortin, A.Kane, R.Owens	65
LES of Non-Newtonian physiological blood flow M.M.Molla, M.C.Paul	69
A three dimensional prototype electro-fluid-structure model of the left ventricle T.N.Croft, D.Carswell, M.Cross, M.Devereux-Cole, A.K.Slone, A.J.Williams	73
Application of viscoelastic constitutive models to blood flow C.B.Liu, P.Nithiarasu	77

MS-3: Computational modelling of respiratory system

Organised by W.A. Wall and K.R. Lutchen

KEYNOTE: Synthesizing imaging and structural models to probe airways and airway structures responsible for asthma K.R.Lutchen, A.Laprod, L.Campana, M.Albert	81
Computational modelling of paranasal sinus gas exchange C.M.Hood, R.C.Schroter, D.J.Doorly	84
Modeling respiratory flow in a CT-scanned upper and lung airway H.Y.Luo, Y.X.Liu, Y.Liu	88
Fluid structure interaction of a human trachea under different ventilation conditions A.Perez del Palomar, M.Malve, M.Doblare	90
Nanoparticle mass transfer in a patient specific human lung A.Comerford, W. A.Wall	94

Simulating pharmaceutical aerosol bolus dispersion and deposition in human upper airways: RANS, LES or DES? S.T.Jayaraju, C.Lacor, S.Verbanck	98
Numerical investigation of the flow field in the upper human airways A.Henze, R.K.Freitas, G.Eitel, W.Schroeder	102
Forcing of low Reynolds number alveolar flows in the lung D.Borer, T.Rösger	107
Integrative modelling of tissue deformation and blood flow distribution in the lung K.S.Burrowes, M.H.Tawhai	111
Surfactant dynamics with SPH S.Adami, X.Y.Hu, N.A.Adams	115
A time varying heterogeneous lung model for airway impedance D.Leary, G.N.Maksym	118
Numerical investigations of the flow in models of the upper central airways L.Krenkel, R.Kessler, C.Wagner	122
Numerical modelling of the air flow in the respiratory tract A.Devys, C.Grandmont, B.Grec, B.Maury, D.Yakoubi	126
High-performance computational modelling of nasal airflow D.J.Taylor, D.J.Doorly, R.C.Schroter, J.Peiro, E.Blenke, R.Almeyda, N.Tolley, G.Houzeaux, M.Vazquez	128
Unsteady flow through a realistic human airway geometry P.H.Saksono, I.Sazonov, P.Nithiarasu	132

MS-4: Wales Institute of Mathematical and Computational Sciences (WIMCS)

Organised by K. Morgan

Investigation of the effects of tensile and compressive loading on the fracture of trabecular bone at the microscale V.L.Kidgell, Y.Feng, O.Hassan	136
Computational requirements of the virtual patient N.W.John, C.J.Hughes, S.R.Pop, F.P.Vidal, O.Buckley	140
Particle methods for a virtual patient O.Buckley, C.Hughes, N.W.John, S.Pop	144
Lattice Boltzmann methods for non-Newtonian fluids G.W.Roberts, D.W.Walker	149
Exact solution to a refined contact problem for biphasic cartilage layers G.Mishuris, I.Argatov	151

MS-5: Cerebral Aneurysm Haemodynamics

Organised by J.R. Cebal and R. Löhner

- Influence of internal carotid artery geometry on aneurysms location and orientation
M.Piccinelli, S.Bacigaluppi, A.Veneziani, A.Remuzzi, L.Antiga 155
- Sensitivity of flow patterns in cerebral aneurysms
J.-D.Müller, M.Jitsumura, N.H.F.Müller-Kronast 159
- Wall shear stress in the Internal Carotid Artery and its relation to aneurysm location
T.Passerini, A.Veneziani, L.M.Sangalli, P.Secchi, S.Vantini 163
- Large-scale CFD in Cerebral Hemodynamics: Characterizing Arterial Flow
G.Houzeaux, R.Aubry, M.Vázquez, H.Calmet, F.Mut, S.Wright, G.Ascoli, J.Cebal 167
- Hemodynamic effects in virtual aneurysm models with stenting
S.Seshadhri, G.Janiga, G.Rose, B.Preim, M.Skalej, D.Thévenin 171

MS-6: Heart-valve modelling

Organised by R. van Loon and X. Luo

- Impacts of Flow Vortex on a Chorded Mitral valve in the Left Ventricle
M.Yi, X.Luo, T.Wang, P.Watton 175
- The analysis of a mechanical heart valve prosthesis and a native venous valve using commercial fluid-structure interaction codes
A.J.Narracott, V.Diaz, D.Rafiroiu, C.Zervides, P.V.Lawford, D.R.Hose 180
- Realistic blood flow through the aortic valve: simulation and analysis
M.Astorino, J.-F.Gerbeau, S.Shadden, I.E.Vignon-Clementel 184
- Heart valve fluid-structure interaction using weak coupling
J.-D.Müller 188
- Towards the development of a numerical method to study FSI of heart valves
A.Joda, J.Fisher, S.Korossis, Z.Jin 190
- Finite element testing in patients' implantation site of new percutaneous pulmonary valve device
C.Capelli, F.Migliavacca, A.M.Taylor, P.Bonhoeffer, S.Schievano 194
- Computational modelling of the beating heart: blood flow through an artificial heart valve
C.Wood, A.Gil, O. Hassan, S. Ashraf 197
- Modelling aortic stenosis
R.van Loon, A.Ionescu 200

MS-7: Recent advances in computational and mathematical methods for imaging and image analysis

Organised by G. Wei

- Image and surface analysis via geometric evolution equations
G.-W.Wei 204

High quality meshing based on harmonic mappings for biomedical simulation
E.Marchandise, J.-F.Remacle, M.Willemet 206

3D reconstruction of a realistic arteriovenous fistula from 2D MRI images: a geometrical remodelling and computational haemodynamics investigation
G.T.Carroll, T.M.McGloughlin, M.T.Walsh 209

MS-8: Methodologies for analysing protein conformational changes

Organised by S. Guest and A. MacDonald

Protein Mechanics
A.Macdonald, S.Guest 213

DynDom3D: a method for the analysis of domain movements in large biomolecular complexes
S.Hayward, G.Poornam, A.Matsumoto, H.Ishida 217

Multi-scale modelling of macromolecular conformational changes
A.Ahmed, H.Gohlke 219

Geometric modeling of flexible motion in proteins
S.A.Wells 223

MS-9: Shape and deformable modelling in biomedical image analysis

Organised by X. Xie and M. Mirmehdi

FFT-Based Conjugate Gradient strategies for numerical simulation of GVF-Snakes
P.Gomo, M.Spann 226

Using shape entropy as a feature to lesion boundary segmentation with level sets
E.M.Massey, A.Hunter, J.A.Lowell, D.Steel 230

A robust active contour approach for studying cell deformation from noisy images
A.Cenedese, A.Silletti 234

Mammographic Image Segmentation using Edge Based Deformable Contour Models
X.Xie 238

Level Set Based Automatic Segmentation of Human Aorta
S.Y.Yeo, I.Sazonov, X.Xie, P.Nithiarasu 242

MS-10: Patient-specific modelling of haemodynamics in aortic aneurysms

Organised by I. Sazonov, P. Nithiarasu and S. Ashraf

Investigations of steady and unsteady flows in an aortic aneurysm
S.Seshadhri, G.Janiga, G.Rose, B.Preim, M.Skalej, D.Thévenin 246

Blood flow through stents in abdominal aortic aneurysms
A.Caiazzo, M.A.Fernández, J.-F.Gerbeau, V.Martin, I.E.Vignon-Clementel 250

Influence of hemodynamics in the formation of an intraluminal thrombus in abdominal aortic aneurysms 254
A.-V.L.B.Salsac, R.Tang, J.C.Lasheras

Axisymmetric and non-axisymmetric flow and wall shear stress in a model fusiform abdominal aortic aneurysm 258
G.J.Sheard

A patient-specific blood flow simulation through an aneurysmal thoracic aorta 262
P.H.Saksono, I.Sazonov, P.Nithiarasu, R.van Loon, H.Luckraz, S.Ashraf

SS-1: Computational electrophysiology

A Riemannian approach to cardiac fiber architecture modelling 269
D.Gil, J.Garcia-Barnes, R.Arís, G.Houzeaux, M.Vázquez

Parallel computational electrophysiology in Cell/B.E. processors 273
F.Rubio, M.Hanzich, R.Arís, G.Houzeaux, M.Vázquez

Application of novel numerical methods to electrophysiology simulation in real heart geometries 276
L.Mirabella, L.Gerardo-Giorda, M.Perego, M.Piccinelli, A.Veneziani, F.Nobile

Numerical methods for accurate and effective simulations in computational electrocardiology 280
L.G.Giorda, M.Perego, A.Veneziani

Analysis of the electro-mechanical activation sequence of the myocardium following the path described by the HVMB 284
J.Marcé-Nogué, F. Roure, G.Fortuny

SS-2: Image processing

Difference imaging of cerebral stroke in the human brain using edge finite element simulations of magnetic induction tomography 288
M.Zolgharni, P.D.Ledger, H.Griffiths

Topological structures in a peripheral bypass graft 292
A.M.Gambaruto, A.Sequeira

Shape matching 296
A.Clark, C.J.Cotter, J.Peiro

Evaluation of optical flow computation techniques to visualize myocardial motion 299
S.Riyadi, M.M.Mustafa, A.Hussain, O.Maskon, I.F.M.Nor

Physical imaging of microcracks in human cortical bone 303
E.Budyn, J.Jonvaux, T.Hoc

SS-3: Modelling fluid-structure interaction in biomedical engineering

Monolithic fluid-solid coupling and applications in the left ventricle D.Nordsletten, M.McCormick, P.Kilner, P.Hunter, D.Kay, N.Smith	307
A numerical acoustic fluid-structure in vivo model of ultrasonic angioplasty in a peripheral artery M.P.Wylie, G.B.McGuinness, G.P.Gavin	312
Accurate prediction of blood flow transients: a fluid-structure interaction approach V.Kanyanta, A.Ivankovic, A.Karac	316
A fluid-structure interaction study of biofilm detachment A.Safari, A.Ivankovic, Z.Tukovic, M.Walter, E.Casey	320
A partitioned matrix-free finite-volume approach to fluid-structure interaction modelling A.G.Malan, O.F.Oxtoby, P.Nithiarasu	324
Fluid-structure interaction in biomedical engineering: a comparison between block Gauss-Seidel and block Newton strategies M.M.Joosten, W.G.Dettmer, D.Peric	328

SS-4: Computational haemodynamics

A finite element approach for static and dynamic simulations of human red blood cells T.Klöppel, W.A.Wall	332
Validation of a numerical model of the hemodynamics in lower-limb bypasses M.Willemet, E.Marchandise, J.-F.Remacle, V.Lacroix	336
Intraventricular and aortic blood flow analysis and reconstruction using the exact solution of non stationary hydrodynamic equations for the class of twisted converging viscous flows G.Kiknadze, A.Gorodkov, A.Bogevolnov	338
Building coupled 3D-1D-0D models in computational hemodynamics P.J.Blanco, M.R.Pivello, S.A.Urquiza, R.A.Feijóo	341
Estimation of contact force distribution between stent and vascular wall to design suitable stent shape D.Yoshino, K.Inoue	345
A lumped parameters model to study left ventricle diseases and to predict surgical therapies V.Gramigna, G.Fragomeni	349
A model of neonatal pulmonary atresia with intact ventricular septum and RV-dependent coronary flow: Can collaterals protect the heart from ischemia? J.P.Mynard, M.R.Davidson, D.J.Penny, J.J.Smolich	353
Evaluation of computational and analytical models for blood perfusion in perforator flaps D.Drikakis, C.Milionis, S.K.Pal, S.Patel, E.Shapiro	357

A model of vascular microbubble transport through a vessel bifurcation A.J.Calderon, B.Eshpuniyani, J.B.Fowlkes, J.L.Bull	361
Computational modelling of left ventricular assist devices D.Carswell, T.N.Croft, D.McBride, A.K.Slone, M.Cross, G.Foster	364
Pulsatile flow investigation in a model Cavopulmonary connection K.Chitra, S.Vengadesan, T.Sundararajan, P.Nithiarasu	368
A new immersed fluid-structure computational framework for haemodynamic applications A.J.Gil, A.Arranz Carreno, J.Bonet, O.Hassan	372
Patient-specific computational modelling of a carotid bifurcation using the Locally Conservative Galerkin (LCG) method R.L.T.Bevan, P.Nithiarasu, R.Van Loon	376

SS-5: Computational tissue mechanics

The effects of external compression on tissue deformation in the lower leg Y.Wang, N.B.Wood, D.N.Firmin, X.Yun Xu	380
Poroviscoelastic anisotropic analysis of the unconfined compression test on articular cartilage S.K.Hoang, Y.N.Abousleiman	384
Characterization of a surrogate lung material made of polyurethane foam and fluid-filled gelatine microcapsules H.K.Parsa, A.Ivankovic, A.Karac	388

SS-6: Modelling diagnosis and treatment procedures

Analysis and optimization of a scoliosis surgical correction procedure J.F.Aguilar Madeira, H. L.Pina, E.B.Pires, J.Monteiro	392
Regularized learning algorithm for prediction of blood glucose concentration in "no action period" S.Pereverzev, S.Sampath	395
Thermal analysis of infant radiant warmer M.Rojczyk, I.Szczygiel	399
A parallelized transient boundary element model of laser hyperthermiaphotodynamic therapy in the oesophagus K.E.Donne, A.Marotin, D.Rees	403

SS-7: Modelling at cellular and molecular level

A molecule dissociation method based on multi-objective optimization K.Yang, X.Wang, H.Jiang	407
--	-----

Molecular dynamics investigation of salt dependent diffusion coefficients for ssDNA oligomers in aqueous solution M.Lai, D.Drikakis	411
Behaviour of tensegrity cells assembly during single cell growth E.W.Postek, R.Smallwood, R.Hose	415
Truss model for stress controlled morphogenesis J.J.Muñoz, V.Conte, M.Miodownik	419

SS-8: Computational biomechanics

Objective balance assessment: female claudicants perform poorly in computerized dynamic posturography K.A.Mockford, F.A.K.Mazari, A.R.Jordan, N.Vanicek, I.C.Chetter, P.A.Coughlin	423
Biomechanical adaptations when landing on football turf P.L.Jones, D.G.Kerwin, G.Irwin, L.D.M.Nokes	427